STABILITY ENHANCEMENT OF THE INTEGRATION OF WIND AND SOLAR ENERGY FED TO SG-BASED POWER SYSTEM

NÂNG CAO ĐỘ ỔN ĐỊNH HỆ THỐNG TÍCH HỢP NĂNG LƯỢNG GIÓ, NĂNG LƯỢNG MẶT TRỜI, NĂNG LƯỢNG TRUYỀN THỐNG KẾT NỐI VỚI LƯỚI

Nguyen Thi Mi Sa, Truong Dinh Nhon
Ho Chi Minh City University of Technology and Education

TÓM TẮT

Bài báo đề xuất một hệ thống điện tích hợp gồm năng lương gió, năng lượng mặt trời và nguồn năng lượng truyền thống kết nối với lưới. Những nguồn năng lượng này có thể kết nối chung với nhau tại bất kì điểm nào trên đường một chiều chung-tạo điều kiện trong việc mở rộng hệ thống trong tương lai. Giải thuật điều khiển dùng kỹ thuật gán cực áp dụng cho bộ nghịch lưu nguồn áp với bộ điều khiển vi tích phân tỉ lệ (PID) được thiết kế để cung cấp các đặc tính giảm chấn phù hợp cho các nghiệm trội của hệ thống dưới nhiều điều kiện vận hành khác nhau. Mô hình tuyến tính hóa sử dụng kỹ thuật quĩ đạo nghiệm dựa trên miền tần số kết hợp với mô hình phi tuyến khi có ngắn mạch 3 pha tại thanh cái chung đều được biểu diễn để minh chứng cho tính hiệu quả của bộ điều khiển được đề xuất.

Từ khóa: *Năng lượng gió, năng lượng mặt trời, năng lượng truyền thống.*

ABSTRACT

This paper proposes an integrated power generation system, applying pole-placement technique, fed by three power sources: wind power, solar power, and traditional power which are connected to a commercial power system. Different power sources can be interconnected anywhere on the same power line, leading to flexible system expansion. The effective control scheme using a voltage source inverter (VSI) joined with a proportional-integral-derivative (PID) damping controller is designed to contribute adequate damping characteristics to the dominant modes of the studied system under various operating conditions. A frequency-domain approach based on a linearized system model using root-loci technique and a time-domain scheme based on a nonlinear system model subject to a three-phase short-circuit fault at the connected bus are systematically performed to examine the effectiveness of the proposed control schemes.

Keywords**:** *Solar power generation, Wind power generation, Fossil fuel steam generator.*

I. INTRODUCTION

Renewable-energy issue is one of the hottest topics in the whole world today due to the fast and huge consumption of fossil fuels. Renewable energy can be derived from several resources such as solar, wind, ocean waves, water flow and tides, geothermal heat, biological sources, etc. [1]. Among these resources, wind power is now a very mature and established renewable energy throughout the world. The use of wind power is increasing at an annual rate of 20%, with a World Wide installed capacity of 238,000 MW at the end of 2011 [2]. However, other renewable energies such as photo voltaic (PV) energy also have significant potential. Since 2004, PVs passed wind as the fastest growing energy, and since 2007 have more than doubled every two

years. The photovoltaic capacity worldwide was 67,000 MW at the end of 2011 [3].

In practice, a hybrid wind and PV energy system can reliably supply a part of the world's energy needs, with significant benefit to climate, air quality, water quality, ecological systems, and energy security, at reasonable cost [4].

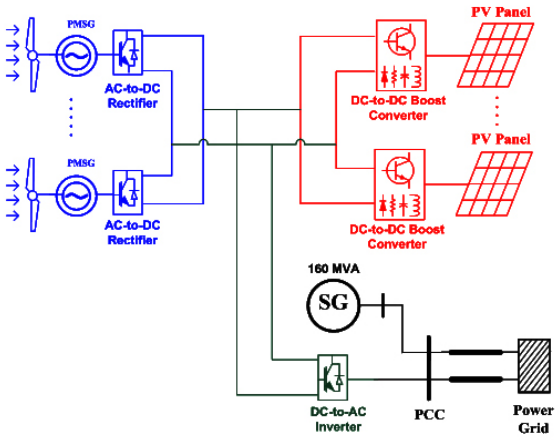

Fig. 1. Configuration of the integration of wind and solar energy generationfed to an SG-based traditional power system.

Nowadays, hybrid system is mainly composed of natural energy sources, and in some cases, it can be incorporated into the system with traditional energy sources like coal and gas well. However, there is a tendency that the greater the system sophistication, the more suitable the power control techniques are required to be.

With this integrated power generation system (i.e., wind power, solar power and traditional power), the strategies for power-fluctuation mitigation and damping improvement are of the vital importance. Among these aspects, PID damping controller using pole-placement technique is the first choice. With this technique, the dominant modes of the studied system can be exactly assigned on the desired locations of the complex plane and the parameters of the PID damping controller can be easily determined [5-6].

This paper presents an effective control scheme using a voltage source inverter (VSI) joined with the PID damping controller to contribute adequate damping to the integrated wind and PV power generation system fed to an SG-based traditional power system under various operating conditions. Frequency-domain approaches based on a linearized system model using Eigen value analysis are performed while time-domain schemes based on nonlinear system models subject to disturbance are also carried out to validate the effectiveness of the proposed control schemes.

II. SYSTEM CONFIGURATION AND MATHEMATICAL MODELS

Fig. 1 illustrates a schematic diagram of the proposed integrated generation consisting of four subsystems: a wind generation subsystem, a solar generation subsystem, an interface subsystem and an SG-based traditional power system. The four subsystems share their DC links.

In the wind generation subsystem, the 5x2-MW wind turbines are represented by five permanent-magnet synchronous generators (PMSG) driven by five variable-speed wind turbines (VSWT) and five rectifiers. The converter is used to control indirectly the operating point of the wind turbine by commanding the rotor speed and the voltage on the PMSG terminals. The dynamic behavior of the wind generation subsystem can be characterized by two nonlinear differential equations involving the *d*- and *q*-axis modulation indices of the VSC-converter. For the detailed mathematic description of the wind subsystem, please refer to [8].

In the solar generation subsystem, there are five photovoltaic (PV) panel arrays and five half-bridge boost DC-DC converters. Similar to the wind subsystem, the converter is used to control the operating point of the PV panels. The dynamic behavior of the solar generation subsystem can be characterized by two nonlinear equations involving the voltage level on the DC-DC converters and the current injected into the DC bus.

These two subsystems are interconnected at the output sides of individual converters and are also connected to the DC-AC inverter through interface subsystem. This inverter converts wind and solar energy generated by these sources useful to costumers.

Three subsystems including wind, solar and interface are also connected to the PCC of the SG-based traditional power system.

The employed mathematical models of the studied system are described as below. The equations in the following subsections are expressed in per unit (pu) except that the time variable t and base angular frequency $\omega_b$are ins and rad/s, respectively.

1. Variable-Speed Wind Turbine

The captured mechanical power P_{mw} (in W)by a VSWT from wind is given by

$$P_{mw} = -\rho_w \cdot A_{rw} \cdot V_w \cdot C_{pw}(\lambda_w, \beta_w) \quad (1)$$

Whereρ_w is the air density (kg/m^3), A_{rw} is the blade impact area (m^2), V_w is the wind speed (m/s), and C_{pw} is the dimensionless power coefficient of the VSWT. The expression for C_{pw} is depicted by

$$C_{pw}(\psi_{kw}, \beta_w) = c_1\left(\frac{c_2}{\psi_{kw}} - c_3 \cdot \beta_w - c_4 \cdot \beta_w^{c_5} - c_6\right) \exp\left(-\frac{c_7}{\psi_{kw}}\right) \quad (2)$$

in which

$$\frac{1}{\psi_{kw}} = \frac{1}{\lambda_w + c_8 \cdot \beta_w} - \frac{c_9}{\beta_w^{\,3} + 1} \quad (3)$$

$$\lambda_w = \frac{R_{bw} \cdot \omega_{bw}}{V_w} \quad (4)$$

Where ω_{hw} is the blade angular speed (rad/s), R_{bw} is the blade radius (m), λ_w is the tip speed ratio, β_w is the blade pit change (degrees), and c_1-$c_9$are the constant coefficients of C_{pw} of the studied VSWT. The cut-in, rated, and cut-out wind speeds of the VSWT are 4,14, and 24m/s, respectively.

2. PMSG Model and Operation of Power Converters

The *d-q* axis equivalent circuit model of the studied wind PMSG can be expressed by [7]

$$p(\phi_{qw}) = \omega_b v_{qsw} + \omega_b r_{sw} i_{qsw} - \omega_{rw} \phi_{dw} \quad (5)$$

$$p(\phi_{dw}) = \omega_b v_{dsw} + \omega_b r_{sw} i_{dsw} + \omega_{rw} \phi_{qw} \quad (6)$$

in which

$$\phi_{qw} = -(X_{mqw} + X_{lsw}) i_{qsw} = -X_{qw} i_{qsw} \quad (7)$$

$$\phi_{dw} = -(X_{mdw} + X_{lsw}) i_{dsw} + X_{mdw} i'_{mw} = -X_{dw} i_{dsw} + X_{mdw} i'_{mw} \quad (8)$$

wheref is the pu flux linkage, v_{sw} is the pu stator-winding voltage, i_{sw} is the pu stator-winding current, X_{mw} is the pu magnetization reactance, X_{lsw} is the pu leakage reactance, i'_{mw} is the pu magnetization current, and w_{rw} is the pu rotational speed of the studied PMSG.

The input *d-q* axispu voltages of the i^{th} VSC-converter of the PMSG can be expressed by $v_{condwi} = km_{condwi} v_{dc}$ and $v_{conqwi} = km_{conqwi} v_{dc}$, respectively, where v_{dc} is the DC-link voltage while km_{condwi} and km_{congwi} are the *d*- and *q*-axis modulation indices of the i^{th}VSC-converter, respectively.

The fundamental control block diagrams of the VSC-based converter of each of the wind PMSG can be referred to [8].In [8],km_{condw} is employed to control the rotor speed of the wind PMSG (w_{rw}), and km_{conqw} is utilized to control the stator-winding voltage of the PMSG (v_{sw}).

3. Model for PV System

Each practical PV panel of the studied system has the following specifications: BP275UU, rated power of 75 W, rated voltage of 17 V, rated current of 4.45 A, open-circuit voltage of 21.4 V, and short-circuit current of 4.5 A. Since the output voltage of PV cell is very low, a number of PV cells are connected together in series in order to obtain required higher voltages. A number of PV cells are put together and encapsulated with glass, plastic, and other transparent materials to protect against harsh environments and a PV module can then be formed. To obtain the required voltage and power, a number of modules are connected in parallel to form a PV array. Fig. 2 shows an equivalent circuit diagram of a

PV array including an equivalent short-circuit current source I_{SC} in parallel with a diode and a shunt resistor R_{sh}, where N_s is the number of cells in series and N_p is the number of modules in parallel. The equivalent-circuit model of the PV array shown in Fig. 2 can be expressed by the following equations [9-10]:

$$I_{PV} = N_p I_{SC} - N_p I_D \left\{ \exp\left[\frac{q}{AkT} \left(\frac{V_{R\_PV}}{N_s} + \frac{R_S I_{PV}}{N_p} \right) \right] - 1 \right\} - \frac{N_p}{R_{sh}} \left(\frac{V_{PV}}{N_s} + \frac{R_S I_{PV}}{N_p} \right) \quad (9)$$

Where V_{R_PV} is the output voltage of the PV array, q is the charge of an electron (q = -1.602×10^{-19} C), k is Boltzmann constant (k = 1.38 ×10^{-23} J/K), T is temperature in K, A is the quality factor which is a constant, I_D is the reverse saturation current of the diode, and I_{SC} is the short-circuit current under the solar radiation of 1000 W/m^2.

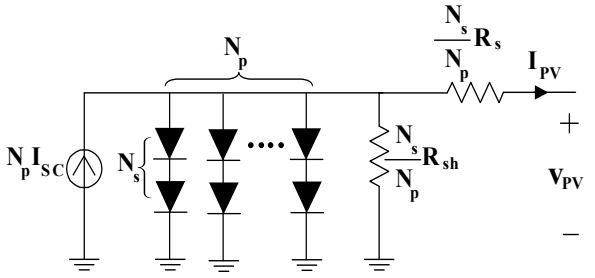

Fig. 2. Equivalent circuit of the studied PV array.

Fig.3 shows that the output voltage of the PV array is fed to a DC-DC boost converter to step up the PV voltage to a higher level. The DC line from the output of the boost DC-DC converter to the input of the DC-AC inverter is represented by an equivalent T circuit as shown in Fig. 4. The capacitor C_{DC}, which is located at the midpoint of the DC line, can be considered as a battery model for energy storage. The dynamic equations of DC-DC boost converter can be expressed by the following gequation:

$$\begin{bmatrix} p(I_L) \\ p(V_C) \end{bmatrix} = \begin{bmatrix} -\frac{R_E + (1-D)(R//R_C)}{L_E} & -\frac{(1-D)R}{L_E(R+R_C)} \\ \frac{(1-D)R}{(R+R_C)C} & -\frac{1}{(R+R_C)C} \end{bmatrix} \begin{bmatrix} I_L \\ V_C \end{bmatrix} + \begin{bmatrix} \frac{1}{L_E} \\ 0 \end{bmatrix} V_{PV} \quad (10)$$

$$V_{R\_PV} = \left[(1-D)(R_C // R) \frac{R}{R+R_C} \right] \begin{bmatrix} I_L \\ V_C \end{bmatrix} \quad (11)$$

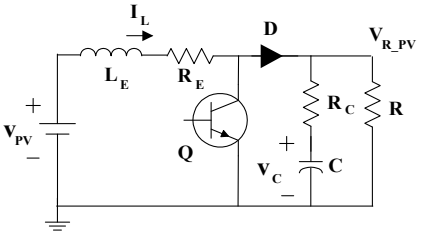

Fig. 3. The equivalent circuit of DC-to-DC boost converter.

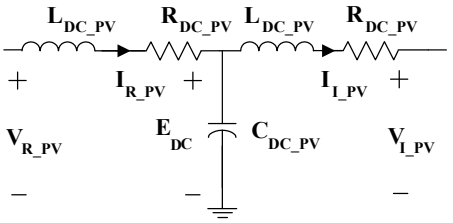

Fig. 4. The equivalent circuit of DC line in PV array.

According to Fig. 4, the pu differential equations of the DC line can be described by

$$(L_{DC\_PV}) p(I_{R\_PV}) = V_{R\_PV} - R_{DC\_PV} I_{R\_PV} - E_{DC} \quad (12)$$

$$(C_{DC\_PV}) p(E_{DC}) = I_{R\_PV} - I_{I\_PV} \quad (13)$$

$$(L_{DC\_PV}) p(I_{I\_PV}) = E_{DC} - V_{I\_PV} - R_{DC\_PV} I_{I\_PV} \quad (14)$$

Fig. 5 shows the control scheme inside the DC-to-AC inverter. The corresponding differential equations for controlling the modulation indices and phase angles of the inverter are described by

$$T_{kminv}.p(\Delta km_{inv}) = K_{kminv}(Q_{w\_pv,ref} - Q_{w\_pv}) - \Delta km_{inv} \quad (15)$$

$$T_{\delta inv}.p(\Delta\delta_{inv}) = K_{\delta inv}(V_{dc\_ref} - V_{dc}) - \Delta\delta_{inv} \quad (16)$$

where Δ represents the quantities of deviation, subscript *ref* denotes the quantities of reference, K_{km} and K_{δ} are the gains of the modulation index control block and the phase angle control block of the inverter,

respectively; and T_{km} and T_{δ} are the time constants of the modulation index control block and the phase angle control block of the inverter, respectively.

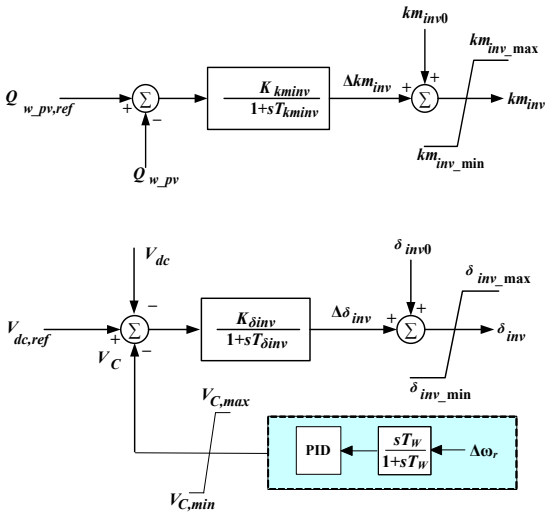

Fig. 5. Control block diagram of DC-to-AC inverter of hybrid system.

4. Interface Subsystem

The DC bus collects the energy generated by both the wind and solar subsystems and delivers it to the utility.

The output *d-q* axis pu voltages of the VSC-inverter of the hybrid system (wind and solar generation) can be written by $v_{invd} = km_{inv} \sin(a_{inv}) v_{dc}$ and $v_{invq} = km_{inv} \cos(a_{inv}) v_{dc}$, respectively, where km_{inv} and δ_{inv} are the modulation index and the phase angle of the VSC-inverter, respectively.

The fundamental control block diagrams of the VSC-based inverter of the hybrid system are shown in Fig. 4.In [8],δ_{inv} is responsible to control the DC-link voltage (v_{dc}), $km_{inv}$is used to control the output reactive power of the hybrid system (Q_{w_pv}), km_{condw} is employed to control the rotor speed of the wind PMSG (w_{rw}), and km_{conqw} is utilized to control the stator-winding voltage of the PMSG (v_{sw}).

5. Synchronous Generator Model

The model and equations for the SG used in this paper are the same as the ones developed in [11].The complete *d*- and *q*-axis equivalent circuits and the corresponding equations of the SG can be referred to [11]. The IEEE type DC1A excitation system (field-controlled DC commutator exciter) is employed in this paper [11]. This SG model takes into account the subtransient effects and is established based on the following assumptions:

(a) The model is established in the *dq*-axis reference frame that is fixed on the rotor and rotates at rotor speed;

(b) The rotor has two windings on each axis, i.e., one field winding and one damper winding on the *d*-axis while two damper windings on the *q*-axis;

(c) The transients of stator and the effects of speed deviation in the stator voltage equations are properly neglected.

III.DESIGN DAMPING CONTROLLERS FOR VSI

This section presents the design of PID damping controllers for the VSI.A unified approach based on modal control theory to design a PID damping controller for modulating the extinction angle γ_I of the inverter is proposed. The PID damping controller employs the speed deviation of the studied SG as a feedback signal to generate a damping control signal V_C in order to improve the damping characteristics of the poorly damped modes (mechanical mode and exciter mode) of the SG.

The procedure and results for designing the PID damping controller of the proposed VSI shown in Fig. 5 are performed to achieve stability improvement of the studied system. The design procedures using a unified approach based on modal control theory can be referred to the ones listed in [12]. The wind speed of 12 m/s for the VSWT of the OWF is properly selected as the nominal operating points for designing the PID damping controller. The values of I_D and I_{SC} PV array

under the irradiance of 1000 W/m^{2}are 9×10^{-11} A and 7.77 A, respectively.

The system eigenvalues of the studied VSI without and with damping controller are listed in the third and fourth column of Table I, respectively. Eigenvalue analysis of the system performed in the steady-state conditions in Table I show that the eigenvalues $\Lambda_{30\text{-}31}$ and $\Lambda_{34\text{-}35}$ have the poorest damping and low-frequency conditions compared with the ones of other modes. The other poor damping of certain high-frequency modes are not considered in this case. Since the amplitude of the high frequency modes die out much faster than the low frequency mode. Moreover, in this paper, the main concerns are stability enhancement of power systems with renewable-energy systems including wind and solar power generation. The capacity of the SG-based power system is significantly large compared with the other ones. These are the reasons why the damping ratios of these two dominant modes need to be improved.

The control block diagram of the VSI including the designed PID damping controller was shown in Fig. 3(a). The first-order wash-out term with the PID controller employs the rotor-speed deviation of the SG ($\Delta\omega_r$) as a feedback signal to generate a damping signal V_C in order to improve the damping ratios of the two dominant modes ($\Lambda_{30\text{-}31}$ and $\Lambda_{34\text{-}35}$) of studied system listed in Table I. The input signal of the PID controller is the rotor-speed deviation $\Delta\omega_r$ while the output signal is the damping signal V_C that is added to the reference DC current V_{Vref}. H(s) is the transfer function of this proposed PID damping controller in s domain and it is from the input signal $\Delta\omega_r$ to the output signal V_C, and s is one of the eigenvalues or poles of the closed-loop system. Hence, this transfer function H(s) is given by

$$\mathrm{H}(s)=\frac{\mathbf{U}(s)}{\mathbf{Y}(s)}=\frac{V_C(s)}{\Delta\omega_r(s)}=\frac{sT_W}{1+sT_W}\left(K_P+\frac{K_I}{s}+sK_D\right) \quad (17)$$

Where T_W is the time constant of the wash-out term while K_P, K_I, and K_D are the proportional gain, integral gain, and derivative gain of the damping controller, respectively. These four unknowns of the PID damping controller can be determined by substituting two pairs of the desired eigenvalues into the characteristic equation of the closed-loop system. The design results are presented as follows.

Table 1. Eigenvalues (rad/s) of the studied system

*denotes the exactly assigned eigenvalues

No.	Subsystem	System without damping controller	System with PID damping controller
$\Lambda_{1\text{-}2}$ $\Lambda_{3\text{-}4}$ $\Lambda_{5\text{-}6}$ Λ_7 Λ_8	PMSG-based OWF	-15.571 ± *j*3.3919×10^6 -15.079 ± *j*3.372×10^6 -2.4039 ± *j*5.6975 -99.298 -100.75	-15.571 ± *j*3.3919×10^6 -15.079 ± *j*3.372×10^6 -2.3841 ± *j*5.68821 -99.298 -100.75
$\Lambda_{9\text{-}10}$ $\Lambda_{11\text{-}12}$ $\Lambda_{13\text{-}14}$ Λ_{15}	PV System	-89.982± *j*90.058 -15.61 ± *j*40.826 -1.5067 ± *j*1.229 -455.42	-89.982± *j*90.059 -15.61 ± *j*40.826 -1.5067 ± *j*1.229 -455.42
$\Lambda_{16\text{-}17}$ $\Lambda_{18\text{-}19}$ $\Lambda_{20\text{-}21}$	Interface System	-311.47 ± *j*2361.8 -17.91 -9.9969	-311.66 ± *j*2361.8 -17.871 -9.997
$\Lambda_{22\text{-}23}$ $\Lambda_{24\text{-}25}$ $\Lambda_{26\text{-}27}$ Λ_{28} Λ_{29} $\Lambda_{30\text{-}31}$ $\Lambda_{32\text{-}33}$ $\Lambda_{34\text{-}35}$	SG-based power System	-21.525 ± *j*106391 -25.492 ± *j*105633 -13.55 ± *j*376.335 -46.379 -37.635 **-0.3591 ± *j*9.3099*** -9.1846 ± *j*11.173 **-0.3803 ± *j*1.2058***	-21.525 ± *j*106391 -25.492 ± *j*105633 -13.55 ± *j*376.335 -46.376 -37.367 **-2 ± *j*9*** -7.0842 ± *j*9.2345 **-1 ± *j*1.2***
Λ_{36}	PID	-	-2.145

Mechanical mode and exciter mode of SG

$\Lambda_{30\text{-}31} = -0.3591 \pm j9.3099$ and $\Lambda_{34\text{-}35} = -0.3803 \pm j1.2058$

Prespecified eigenvalues

$\Lambda_{30\text{-}31} = -2.0 \pm j9.0$ and $\Lambda_{34\text{-}35} = -1.0 \pm j1.2$

Parameters of the designed PID damping controller

$K_P = -0.45$, $K_I = 49.88$, $K_D = 0.22$, and $T_W = 0.31$s

The eigenvalues of the studied system with the proposed VSI joined with the designed PID damping controller are listed in the fourth column of Table I. It can be clearly observed that both modes $\Lambda_{30\text{-}31}$ and $\Lambda_{34\text{-}35}$ have been exactly positioned on the desired locations on the complex plane. The damping ratios of modes $\Lambda_{30\text{-}31}$ and $\Lambda_{34\text{-}35}$ have also been increased from 0.0385to 0.2169and from 0.3008to 0.6402, respectively. Some major constraints for selecting the assigned eigenvalues can be referred to [12]. According to the eigenvalue results listed in the fourth column of Table I and the four parameters of the designed PID damping controller of the VSI shown above, it can be concluded that the design results are appropriate to the studied system.

IV. TIME-DOMAIN SIMULATIONS

This section employs the nonlinear-system model developed in Section II to compare the damping characteristics contributed by the proposed VSI joined with the designed PID damping controller on stability improvement of the studied system under a three-phase short-circuit fault at the infinite bus. It is assumed that the OWF operates under a wind speed V_W of 12 m/s, the PV array operates under the irradiance of 1000 W/m^2, the short-circuit current I_{SC} of 7.77 A, and the diode's reverse saturation current I_D of 9×10^{-11} A. Simulation results of the studied system subject to a three-phase short-circuit fault using MATLAB/ Simulink toolbox are presented in Fig. 6. The fault is suddenly applied to the infinite bus at t = 3 s and is cleared at t = 3.1s. Fig.6 plots the comparative transient responses of the proposed VSI without damping controller (blue lines) and with the designed PID damping controller (red lines). It is clearly observed from the comparative transient simulation results shown in Fig.6 that the proposed VSI joined with the designed PID damping controller can offer better damping to the studied system.

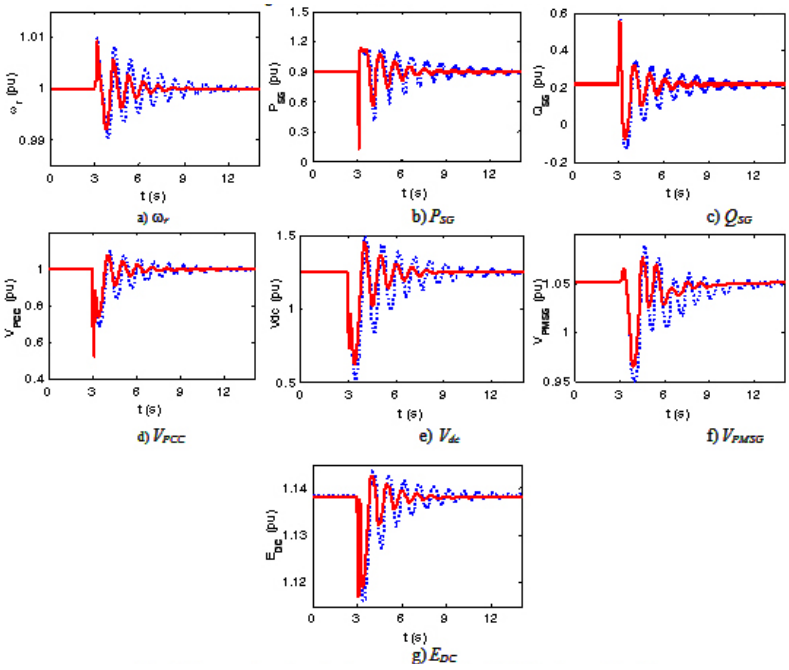

Fig. 6. Comparative transient responses of the studied system subject to a three-phase short-circuit fault at the infinite bus.

In Fig. 6, the important quantities of the SG such as rotor speed (ω_{SG}), output active power (P_{SG}) and output reactive power (Q_{SG}) are shown in Figs. 6(a)-6(c), respectively. The comparative responses of the voltage at PCC (V_{PCC}) and DC voltage (V_{dc}) are shown in Figs. 6(d)-6(e), respectively. The terminal voltage (V_{PMSG}) of the equivalent aggregated PMSG-based OWF are presented in Fig. 6(f). Finally, the voltage of DC line of the PV system (E_{DC}) is shown in Fig. 6(g). It is obviously seen that, without damping controller, the damping of the studied system is so poor and the settling time is about 12 s. By adding the designed PID damping controller to the VSI, the system has better damping and the settling time is about 7 s. It means that the proposed VSI with the designed PID damping controller can offer better damping characteristics to quickly damp out the inherent oscillations of the studied system than the studied system without damping controller.

V. CONCLUSION

This paper has presented the stability improvement of an integration of an OWF and a PV system fed to an SG-based traditional power system. To achieve the power - fluctuation mitigation and damping improvement of the studied system, a PID damping controller for the VSI has been designed. Comparative time - domain simulations of the studied system subject to a three-phase short-circuit fault at the infinite bus have been performed to demonstrate the effectiveness of the VSI joined with the designed damping controller on suppressing inherent oscillations of the studied system under the severe three-phase short-circuit fault.

REFERENCES

[1] U. Bossel, "On the way to a sustainable energy future," in *Proc.27th International Telecommunications Conference (INTELEC)*, Berlin, Germany, Sep. 18-22, 2005, pp. 659-668.

[2] REN21, "Renewables 2011 global status report," Paris, 2011.

[3] European Photovoltaic Industry Association, "Market report 2011," 2012.

[4] M. A. Delucchi and M. Z. Jacobson, "Providing all global energy with wind, water, and solar power, Part I: Technologies, energy resources, quantities and areas of infrastructure, and materials," *Energy Policy*, vol. 39, no. 3, pp. 1154-1169, Mar. 2011.

[5] L. Wang and M. S.-Nguyen Thi, "Stability analysis of four PMSG-based offshore wind farms fed to an SG-based power system through an LCC-HVDC link," *IEEE Transactions on Industrial Electronics,* vol. 60, no. 6, pp. 2392-2400, Jun. 2013.

[6] L. Wang and M. S.-Nguyen Thi, "Comparisons of damping controllers for stability enhancement of an offshore wind farm fed to an OMIB system through an LCC-HVDC link," *IEEE Transactions on Power Systems,* vol. 28, no. 2, pp. 1870-1878, May 2013.

[7] L. Wang and C.-N. Li, "Dynamic stability analysis of a tidal power generation system connected to an onshore distribution system," *IEEE Trans. Energy Conversion*,vol. 26, no. 4, pp. 1191-1197, Dec. 2011.

[8] L. Wang and J.-H. Liu, "Dynamic analysis of a grid-connected marine-current power generation system connected to a distribution system," *IEEE Trans. Power Systems*, vol. 25, no. 4, pp. 1798-1805, Nov. 2010.

[9] M. A. Mahmud, H. R. Pota, and M. J. Hossain, "Dynamic stability of three-phase grid-connected photovoltaic system using zero dynamic design approach," *IEEE Journal of Photovoltaics*, vol. 2, no. 4, pp. 564-571, Oct. 2012.

[10] C.-H. Lin, W.-L. Hsieh, C.-S. Chen, C.-T. Hsu, T.-T. Ku, and C.-T. Tsai, "Financial analysis of a large-scale photovoltaic system and its impact on distribution feeders," *IEEE Trans. Industry Applications*, vol. 47, no. 4, pp. 1884-1891, Jul./Aug. 2011.

[11] P. M. Anderson and A. A. Fouad, *Power System Control & Stability*, Chapters 4-6, Iowa: The Iowa State University Press, Ames, 1977.

[13] L. Wang, K.-H. Wang, W.-J. Lee, and Z. Chen, "Power-flow control and stability enhancement of four parallel-operated offshore wind farms using a line-commutated HVDC link," *IEEE Trans. Power Delivery*, vol. 25, no. 2, pp. 1190-1202, Apr. 2010.